A MLPG Meshless Method for Numerical Simulation of Unsteady Incompressible Flows

I. Saeedpanah

Department of Civil Engineering, Faculty of Engineering, University of Zanjan, Zanjan, Iran.

Email: Saeedpanah@Znu.ac.ir

ABSTRACT

This article presents a numerical algorithm using the Meshless Local PetrovGalerkin (MLPG) method for numerical simulation of unsteady incompressible flows, governed by the Navier–Stokes equations via the stream function–vorticity *(ψ–ω)* formulation. The driven flow in a square cavity is used as the model problem. The present method is a truly meshless method based only on a number of randomly scattered nodes. The multiquadrics RBFs are employed for constructing trial functions in the local weighted meshless local Petrov–Galerkin method. The present numerical algorithm is based on a local weighted residual method with the Heaviside step function as the test function over a local subdomain. The efficiency, accuracy and robustness of the numerical algorithm are demonstrated by the standard driven cavity. It is observed that the obtained results agreed very well with the results of Ghia. Therefore the ability and accuracy of the present numerical algorithm was presented by solving the standard driven cavity flow problem with reasonable accuracy when compared to solutions obtained by Ghia. In other words the benchmark computations indicate that the MLPG Meshless method is very effective in the simulation of fluid flow problems.

NOMENCLATURE

C, η, β	shape parameters	α_Q	dimensionless size of quadrature domain
d_c	characteristic length between node i and its neighbor nodes	α_s	dimensionless size of support domain
n	number of nodes in the support domain	μ	dynamic viscosity
r_s	radius of the support domain	$u^h(y,z)$	radial basis functions
r_Q	radius of the quadrature domain (subdomain)	Γ_Q	boundary of the quadrature domain
Re	Reynolds number	Ω_Q	quadrature domain (local subdomain)
t	time	Ω_s	support (interpolation) domain for point xQ
u	component of velocity in the x direction	ρ	density of the fluid
v	component of velocity in the y direction	$\phi(x)$	shape function
W	heaviside step weight function	ω	vorticity
		α_c	dimensionless shape parameters for MQ
		ψ	stream function

1. INTRODUCTION

Due to the limitations of physical models such as the lack of adequate instruments and also problems due to the lack of complete similarity with real flow, obtaining laboratory results for most of the practical cases is not possible. Regarding these problems and advancement of computers, a method which is commonly used in recent years for flow analysis, is computational fluid dynamics. Unlike the experimental simulations, flow conditions and the dimensions of the domain in these schemes could easily be changed in order to fulfill the design and study purposes. One of the most important problems in the field of computational fluid dynamics is solution of the governing equations, which describes the incompressible fluid flow. Therefore the fluid flow behavior can be studied by solving the Navier-Stokes equations using numerical methods. Incompressible Navier–Stokes flow in two dimensions is one of severalmajor problems in fluid mechanics that have

been extensively studied both theoretically and numerically. The numerical methods such as finite difference method (Jafari *et al*. 2011), finite volume method (Shirani *et al*. 2011; Harichandan and Roy 2012), and finite element method (Bunsri *et al*. 2008; Alam *et al*. 2016), are generally used. These methods have widely been used in computational fluid dynamics for solving the governing equations of flow field as the most important subjects in computational fluid dynamics. Therefore there are numbers of well known conventional numerical methods (Finite Element Method, Finite Volume Method and Finite Difference Method) but Finite Element Method (FEM), because of its versatility and flexibility is extensively used as an analysis tool in various engineering applications. However, on the other hand FEM suffers from drawbacks such as locking problem, element distortion, and loss in accuracy and the need for remeshing. The finite element method (FEM) has been established as a very powerful numerical technique for the analysis of space domain problems having arbitrary shapes. But it has some drawbacks. It has been observed that in the finite element method, mesh generation is a far more time-consuming and expensive task than the assembly and solution of the finite element equations. Moreover, there are certain classes of problems for which FEM is difficult, or even impossible to apply, like problems with discontinuities, moving boundaries, or severe deformations. For such problems, it has become necessary to find the methods, which may be somewhat more expensive from the viewpoint of computer time but require less time in the preparation of data. Meshless methods for numerical solutions of boundary value problems have generated much attention in recent years. In other words recently, a class of new methods, known as meshless methods, has been developed. Therefore development of efficient computational approaches for the numerical simulation of the steady and the unsteady viscous fluid flow has become a very important need in various fields of practical engineering. There are also recent developments in the applications of meshless techniques to fluid flow and groundwater flow problems (Saeedpanah *et al*. 2011). The meshless methods are an extensive area of research for solving CFD problems. Therefore meshless methods were established with the objective of eliminating the requirement of mesh generation step, which is time-consuming and burdensome, in FEM. Owing to these reasons, meshless methods have received much attention as a number of meshless methods have been introduced by different authors. These include smooth particle hydrodynamics (Chen *et al*. 2015; Monaghan 1992), reproducing kernel particle method (Liu *et al*. 1995), the method of finite spheres (De and Bathe 2000), local boundary integral equation (LBIE) method (Zhu *et al*. 1998), the partition of unity method (Babuska and Melenk 1997), element-free Galerkin (EFG) method (Belytschko *et al*. 1994; 1996; Lu *et al*. 1994; Dolbow and Belytschko 1998), meshless local Petrov–Galerkin (MLPG) method (Atluri and Zhu 1998a; Atluri and

Zhu 1998b; Atluri and Shen 2002; Gu YT and Liu GR 2001), natural element method (Sukumar *et al*. 1998), etc. The methods based on global weak form showed promising results but they suffer a drawback. They are not truly meshless methods, i.e. they are 'meshless' only in termsof the interpolation of the field variables and have to use background cells to integrate a weak form over the problem domain. The MLPG method does not need any 'element' or 'mesh' for either field interpolation or background integration, and any non-element interpolation scheme such as the MLS, the PUM, or the RBFs can be used for trial and test functions. The flexibility in choosing the size and the shape of the local sub-domain leads to a convenient formulation in dealing with non-linear problems. The subdomain can be any simple geometry such as circles, rectangles, or ellipses centered at the field node in question in two dimensions. Therefore the meshless local Petrov-Galerkin (MLPG) method is a truly meshless method, which requires no elements or background cells, for either the interpolation or the integration purposes. The concept of MLPG was first proposed by Atluri and Zhu (1998a; 1998b), and later discussed in depth in Atluri and Shen (2002). Remarkable successes of the MLPG method in computational mechanics have been reported in recent years. The MLPG method was first applied to solve the incompressible flow equations by Lin and Atluri (2001). Lin and Atluri (2001) used the MLPG method to solve the Stokes flow and the lid-driven cavity flow problems. In their work, the governing equations were based on the primitive-variables formulation, but in the present work the formulation is based on two equations including stream function Poisson equation and vorticity advection-dispersion-reaction equations. As respects the advantages in using the vorticity-stream function formulation for two-dimensional computations are well known, then two equations, vorticity transport and streamline poisson equations are treated separately via their formulation in advance and their behaviors are investigated. The present numerical algorithm is based on a local weighted residual method with the Heaviside step function as the test function over a local subdomain. The multiquadrics RBFs are employed for constructing trial functions in the local weighted meshless local Petrov–Galerkin method. The driven cavity flows offer an ideal framework in which meaningful and detailed comparisons can be made between results obtained from experiment, theory, and computation. In fact, as hundreds of papers attest, the driven cavity problem is one of the standards used to test new computational schemes. Another great advantage of this class of flows is that the flow domain is unchanged when the Reynolds number is increased. Finally, the ability and accuracy of the present numerical algorithm was presented by solving the standard driven cavity flow problem with reasonable accuracy when compared to solutions obtained by Ghia (1982). In other words the benchmark computations indicate that the MLPG Meshless method is very effective in the simulation of fluid flow problems.

2. RADIAL BASIS FUNCTION (RBF) INTERPOLATION

In recent years, many numerical methods based on the radial basis functions have been introduced and improved for solving several types of computational fluid dynamics problems. The numerical methods based on the radial basis functions are truly meshless methods because these methods depend on a scattered set of nodes in the domain and they do not require any extra information. Therefore, these types of numerical techniques could be easily employed for dealing with high dimensional problems or models with complex geometric domain. This is the main advantage of numerical methods based on the radial basis functions. Meshless methods using radial basis functions have been gained quite importance due to their simplicity and straightforward implementation, and they are becoming a viable alternative as a method for the numerical solution of partial differential equations. The MLPG meshless method requires a local non-element type interpolation or approximation to represent the trial function. The local approximation schemes like MLS, PUM, and RKPM use fictitious values at scattered nodes, and the local interpolation using RBFs enable trial functions that pass through the actual values of the unknown variables at scattered nodes, the later one is used in this present work. Consider a continuous function u(x) defined in a domain Ω, which is represented by a set of field nodes. The u(x) can be interpolated from the neighboring n nodes that are located in the gauss point xQ support domain by using radial basis functions as:

$$u^h(X, X_Q) = \sum_{i=1}^{n} g_i(X) \overline{a}_i(X_Q) = G^T(X) a(X_Q) \quad (1)$$

where $g_i(x)$ is the radial basis function in the space coordinates $x^T=[y,z]$, n is the number of nodes in the neighborhood (refers to the domain of interpolation) of x_Q, and $\overline{a}_i(x_Q)$ are the coefficients for $g_i(x)$, respectively, corresponding to the given point x_Q. It should be noted that the number *(n)* of the neighboring nodes of x_Q is less than or equal to the total number of nodes in the global problem domain *(n_t)* depending on the size of support domain specified. The vectors are defined as:

$$\overline{a} = [\overline{a}_1, \overline{a}_2, \overline{a}_3, ... \overline{a}_n]^T \quad (2)$$

$$G^T = [g_1(X), g_2(X), g_3(X), ..., g_n(X)]^T \quad (3)$$

The radial distance function in a vertical two dimensional domain is a function of Euclidean distance r defined as:

$$r_i = \left[(y - y_i)^2 + (z - z_i)^2 \right]^{\frac{1}{2}} \quad (4)$$

The radial distance function transforms a multiple dimensional problem into one dimension. Enforcing the interpolation to pass through all *n* scattered points within the point x_Q support domain leads to the following set of equations for the coefficients $\overline{a}_i(x_Q)$:

$$u_k = u(y_k, z_k) = \sum_{i=1}^{n} \overline{a}_i(X_Q) g_i(y_k, z_k), k = 1,2,3,...,n \quad (5)$$

which can be expressed in matrix form as follows:

$$Aa = U_s \quad (6)$$

Where $U_s = [u_1, u_2, u_3, ..., u_n]$ and A is the interpolation matrix of rank $(n \times n)$ as follows:

$$A = A^T = \begin{bmatrix} g_1(r_1) & g_2(r_1) & \cdots & g_n(r_1) \\ g_2(r_2) & g_2(r_2) & \cdots & g_n(r_2) \\ \vdots & \vdots & \ddots & \vdots \\ g_1(r_n) & g_2(r_n) & \cdots & g_n(r_n) \end{bmatrix} \quad (7)$$

The coefficients can be obtained as:

$$a = A^{-1} U_s \quad (8)$$

where A^{-1} is the inverse matrix of *A*. Finally, the interpolation can be expressed as:

$$u^h(X) = G^T(X) A^{-1} U_s = \Phi(X) U_s \quad (9)$$

where A^{-1} is the inverse matrix of *A*. Finally, the interpolation can be expressed as:

$$\Phi(X) = [\phi(X), \phi_2(X), \phi_3(X), ..., \phi_k(X), ..., \phi_n(X)] \quad (10)$$

in which

$$\phi_k(X) = \sum_{i=1}^{n} g_i(X) \overline{A}_{i,k} \quad (11)$$

and $\overline{A}_{i,k}$ is the (*i,k*) element of the matrix A^{-1}. The derivatives of $\phi_k(x)$ can be obtained as follows:

$$\frac{\partial \phi_k}{\partial y} = \sum_{i=1}^{n} \frac{\partial g_i}{\partial y} \overline{A}_{i,k} \quad (12)$$

$$\frac{\partial \phi_k}{\partial z} = \sum_{i=1}^{n} \frac{\partial g_i}{\partial z} \overline{A}_{i,k} \quad (13)$$

There are several radial basis functions available. The most important three *RBFs* consisting Multiquadrics (*MQ*), Gaussian (*EXP*) and thin plate splines (*TPS*) are as follows (Franke 1982; Kansa 1990; Hardy 1990).

$$g_i(y, z) = (r_i^2 + C^2)^{\beta} \quad (14)$$

$$g_i(y, z) = (r_i)^{\eta} \log r_i \quad (15)$$

$$g_i(y, z) = e^{-e^2 r_i^2} \quad (16)$$

where β, *C* and η are shape parameters that are used for fine tunning. The partial derivatives of these *RBFs* can be obtained as follows:

$$\frac{\partial g_i}{\partial y} = 2\beta (r_i^2 + C^2)^{\beta-1} (y - y_i) \quad (17)$$

$$\frac{\partial g_i}{\partial z} = 2\beta (r_i^2 + C^2)^{\beta-1} (z - z_i)$$

$$\frac{\partial g_i}{\partial y} = \frac{1}{r_i} (\eta \ln r_i + 1) r_i^{\eta-1} (y - y_i) \quad (18)$$

$$\frac{\partial g_i}{\partial z} = \frac{1}{r_i}\left(\eta \ln r_i + 1\right) r_i^{\eta-1}\left(z - z_i\right)$$

$$\frac{\partial g_i}{\partial y} = -2c^2 e^{-e^2 r_i^2}\left(y - y_i\right) \qquad (19)$$

$$\frac{\partial g_i}{\partial z} = -2c^2 e^{-e^2 r_i^2}\left(z - z_i\right)$$

Multiquadrics RBFs (Eq. (14)) and partial derivatives of these RBFs (Eq. (17)) are used here. Therefore the *MQ* method is a special version of the radial basis functions method. In 1982 Franke tested a large number of interpolation methods for two dimensional scattered data, and found that *MQ* method was one of the most impressive. Also, according to Kansa and Hardy (1990) for its good performance in many cases we choose *MQ* as the radial basis function in this paper. Fig. 1 shows typical shape functions for two-dimensional problem using *MQ* basis with an interpolation domain containing *5*5* nodes.

3.   GOVERNING EQUATIONS

As seen in Fig. 3 the plate is moving with horizontal velocity *U*. As a result the flow field is not a surface flow. Consequently the terms relating to the Froude number vanish. Hence the general non-dimensional, non conservative form of the Navier-Stokes equations in a two dimensional problem in Cartesian coordinates system can be written as:

$$\frac{\partial u}{\partial t} = \frac{1}{\text{Re}}\left[\frac{\partial^2 u}{\partial x^2} + \frac{\partial^2 u}{\partial y^2}\right] - u\frac{\partial u}{\partial x} - v\frac{\partial u}{\partial y} - \frac{\partial p}{\partial x} \qquad (20)$$

$$\frac{\partial v}{\partial t} = \frac{1}{\text{Re}}\left[\frac{\partial^2 v}{\partial x^2} + \frac{\partial^2 v}{\partial y^2}\right] - u\frac{\partial v}{\partial x} - v\frac{\partial v}{\partial y} - \frac{\partial p}{\partial x}$$

$$\frac{\partial u}{\partial x} + \frac{\partial v}{\partial y} = 0$$

where *u* and *v* are the velocities in *x* and *y* direction respectively, *p* is the pressure, *Re* is the Reynolds number. With regard to the selected formulation, a specific numerical method should be taken, so that, pressure-velocity interfere is achieved. So, for the solution of the Navier–Stokes equations, it is essential to use a suitable form of the equations concerning the discretization of the domain and the boundary conditions. The dimensionless non conservative two-dimensional Navier–Stokes equations in stream function–vorticity *(ψ–ω)* formulation within closed domains in Cartesian coordinate system are as follows:

$$\frac{\partial \omega}{\partial t} + u\frac{\partial \omega}{\partial x} + v\frac{\partial \omega}{\partial y} = \frac{1}{\text{Re}}\left[\frac{\partial^2 \omega}{\partial x^2} + \frac{\partial^2 \omega}{\partial y^2}\right] \qquad (21)$$

where *ω, ψ* and *Re* are the vorticity, the stream function and Reynolds number. The velocity components along *x* and *y* directions are denoted by *u* and *v*, respectively and are related with *ψ* and *ω* as follows:

$$u = \frac{\partial \psi}{\partial y}; v = -\frac{\partial \psi}{\partial x}; \omega = \frac{\partial v}{\partial x} - \frac{\partial u}{\partial y} \qquad (22)$$
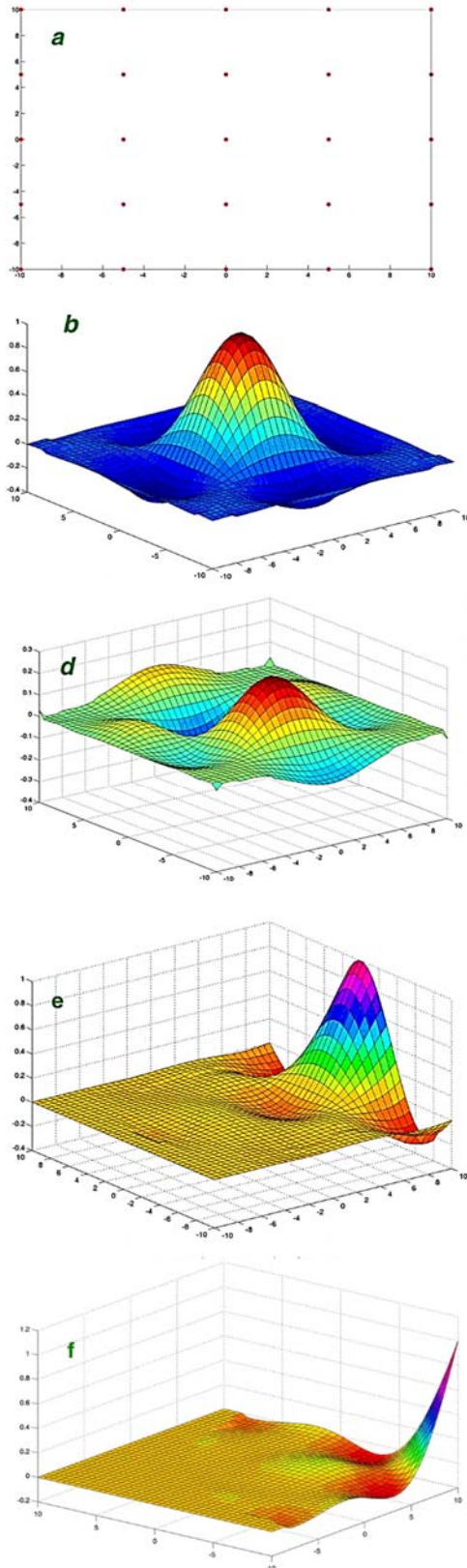

Fig. 1. Shape functions for two-dimensional domain (25 nodes). a) Domain and nodal arrangement, b) shape function of central node, c) shape function derivative in *x* direction of central node, d) shape function derivative in *y* direction of central node, e) shape function for an edge node, f) shape function for a corner node.3.

In the above equations, $Re = UL/\upsilon$,where υ is the kinematic viscosity. One of the advantages of using stream function–vorticity $(\psi–\omega)$ formulation lies in removing pressure gradient terms from the solution process, resulting in a higher numerical stability of the computational scheme. The pressure does not appear in the solution procedure and has no influence on the velocity field, a fact that is of course valid only for incompressible fluid approximation. The pressure can be computed after velocity field is being solved by the Poisson pressure equation:

$$\frac{\partial^2 p}{\partial x^2} + \frac{\partial^2 p}{\partial y^2} = 2\left[\left(\frac{\partial^2 \psi}{\partial x^2}\right)\left(\frac{\partial^2 \psi}{\partial y^2}\right) - \left(\frac{\partial^2 \psi}{\partial x \partial y}\right)^2\right] \quad (23)$$

4. DISCRETIZATION

Meshless methods which use weak form of equations are categorized into global weak form and local weak form. EFG and RKPM are examples of global weak methods over entire domain Ω whereas MLPG uses local weak form of equations over a local sub-domain of arbitrarily shaped Ω_Q called quadrature domain, which is located entirely inside the global domain Ω.This is the most distinguishing feature of the MLPG. In comparison to global weak form methods, local weak form will provide a clear concept for a local meshless integration of the weak form, which does not need any background integration cells over the entire domain. Also, it will lead to a natural way to construct the global stiffness matrix: not through the integration over a contiguous mesh, and by assembly of the stiffness matrices of the elements in the mesh, but through the integration over local sub-domains.

4.1 Discretization of the Poisson Equation

The 2-D Poisson equation of streamline with boundary conditions is as follows:

$$\frac{\partial^2 \psi}{\partial x^2} + \frac{\partial^2 \psi}{\partial y^2} = \omega \quad (24)$$

$$\psi_i = \overline{\psi_i} \, on\Gamma_\psi, \frac{\partial \psi}{\partial n}\bigg|_i = \overline{t} \, on\Gamma_t$$

where ω is treated as a given source function, and thedomain Ω is enclosed by $\Gamma = \Gamma_\psi \cup \Gamma_t$, Γ_ψ is the essential boundary conditions, Γ_t is given, n is the outward unitnormal vector to Γ, Γ_ψ and Γ_t are subsets of Γ satisfying $\Gamma_\psi \cap \Gamma_t = 0$ and $\Gamma_\psi \cup \Gamma t = \Gamma$. As shown in Fig. 2 in the MLPG method, the local weak form of the Petrov-Galerkin residual formulation is used over a local quadrature domain Ω_Q to establish discrete system equations. An arbitrarily shaped support domain can be used. Generally, a circle or rectangular support domain is used for convenience. A general weak form of Eq. (24) by applying the weighted residual method locally over the quadrature domain can be written as:

$$\int_{\Omega_Q} W\left(\frac{\partial^2 \psi}{\partial x^2} + \frac{\partial^2 \psi}{\partial y^2} - \omega\right) d\Omega = 0 \quad (25)$$
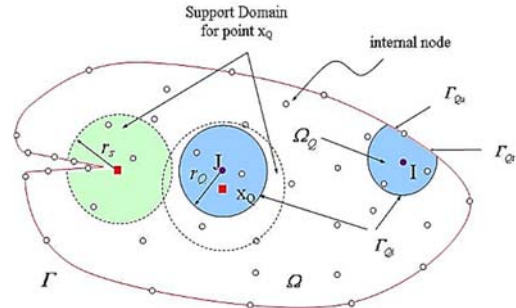

Fig. 2. The support domain and quadrature domain in constructing the discretized equation for node I.

where ψ is the trial function and W is the test function. Using the divergence theorem, we obtain the local weak form as:

$$\int_{\Omega_Q}\left(\frac{\partial W}{\partial x}\frac{\partial \psi}{\partial x} + \frac{\partial W}{\partial y}\frac{\partial \psi}{\partial y}\right)d\Omega - \int_{\Gamma_Q} W\frac{\partial \psi}{\partial n}d\Gamma \quad (26)$$
$$+ \int_{\Omega_Q} W\omega d\Omega = 0$$

in which Γ_Q is the boundary of the quadrature domain Ω_Q and n is the outward unit normal to the boundary Γ_Q. Imposing the natural boundary condition, Eq. (26), we obtain

$$\int_{\Omega_Q}\left(\frac{\partial W}{\partial x}\frac{\partial \psi}{\partial x} + \frac{\partial W}{\partial y}\frac{\partial \psi}{\partial y}\right)d\Omega - \int_{\Gamma_{Qu}} W\frac{\partial \psi}{\partial n}d\Gamma \quad (27)$$
$$- \int_{\Gamma_{Qi}} W\frac{\partial \psi}{\partial n}d\Gamma = \int_{\Gamma_{Qt}} W\overline{t}d\Gamma - \int_{\Omega_Q} W\omega d\Omega$$

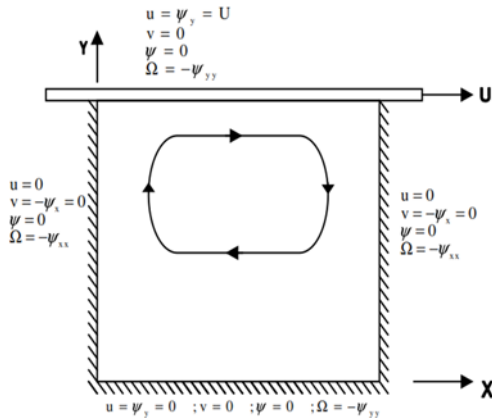in which Γ_{Qt} is a part of Γ_Q, over which the natural boundary condition is specified; Γ_{Qu} is the intersection of Γ_Q and the essential boundary Γ_u; Γ_{Qi} is the internal part of Γ_Q on which no boundary condition is specified, as shown in Fig. 2. For a quadrature domain located entirely within the global domain, there is no intersection between Γ_Q and Γ, and the integrals over Γ_{Qu} and Γ_{Qt} vanish. As shown in Fig. 2 Ω_Q is the local test or weight function domain where $w \neq 0$ (size r_Q). Different local test functions can be used in the weak form (Eq. 27) which leads to different ways to construct the global stiffness matrix (Liu 2003). In fact, the MLPG method is a fundamental base for the derivation of many meshless formulations, since trial and test functions are chosen from different functional spaces. There are many options for the test function (Atluri and Shen 2002). One of these is the Heaviside step function. The Heaviside step test function maintains a unit value at the node and gives zero value at all other nodes. The feature makes the evaluation of the integrals and therefore the whole procedure more efficient. This is a big advantage of the Heaviside step test function. The formulation based on this test function is also one of most accurate methods among all options available so far, according to numerical investigations made in reference (Atluri and Shen 2002). In order to simplify in the weak form (Eq. 27), I deliberately select a test function W such that it vanishes on Ω_Q. This can be easily accomplished by using the

Heaviside step function as the weight function, with the radius r_w of the support of the weight function being replaced by the radius r_Q of the local domain Ω_Q, such that the domain integral vanishes. Therefore in this research in order to avoid the evaluation of any numerical integration in the weak form (Eq. 27), the Heaviside step test function is chosen as the test function in each sub-domain. Using the Heaviside step function as test function, the local weak form (Eq. 27) can be rewritten as:

$$-\int_{\Gamma_{Qu}} \frac{\partial \psi}{\partial n} d\Gamma - \int_{\Gamma_{Qi}} \frac{\partial \psi}{\partial n} d\Gamma = \int_{\Gamma_{Qt}} \bar{t} d\Gamma - \int_{\Omega_Q} \omega d\Omega \qquad (28)$$

Fig. 3. The cavity and its corresponding boundary conditions.

It should be noted that because the system equations are established node by node, the process of assembly of the stiffness matrix is similar to that in the finite-difference method. That is, the entries in the ith row of the stiffness matrix are just the coefficients of the equation defined at node i. The use of the local weak form. for one node will yield only one linear equation involving $\hat{\psi}$. Note that the trial function u within the quadrature domain Ω_Q, in the RBF interpolation, is determined by the fictitious nodal values, $\hat{\psi}$ within the "support domain" for all gauss points x_Q falling within Ω_Q. The local weak form. Eq. (28), gives one algebraic equation relating all these $\hat{\psi}_i$. Thus, one obtains as many equations as the number of nodes. Therefore, we need as many local domains Ω_Q as the number of nodes in the global domain to obtain as many equations as the number of unknowns. In the present implementation, the local domain is chosen as a circle, centered at a node x_i. To obtain the discrete equations from the local weak form. (28), the RBF (9) is used to interpolation the trial function ψ. Substitution of Eq. (9) into Eq. (28) for all nodes leads to the following discretized system of linear equations:

$$[K]\{\psi\} = \{f\} \qquad (29)$$

where, the entries of the "stiffness" matrix K and the "load" vector are defined by

$$[K]_{ij} = \int_{\Omega_Q} \phi_{j,k}(X) W_{,k}(X, X_i) d\Omega \qquad (30)$$

$$-\int_{\Gamma_{Qu}} \frac{\partial \phi(X)}{\partial n} W(X, X_i) d\Gamma$$

$$\{f\}_i = \int_{\Gamma_{Qu}} \bar{t}(X) W(X, X_i) d\Omega \qquad (31)$$

One can easily notice that the numerical integration in one local sub-domain gives two equations, without any global background integration mesh. Gauss quadrature is employed in each local sub-domain centred at node x_i. For each Gauss quadrature point x_Q, RBF is performed to obtain the integrand. Therefore, for a node x_i, there are two local domains: the test function domain Ω_{te} for $Wi\neq0$ (size r_Q), and the interpolation domain Ω_s for x_Q (size r_s). Fig. 2 shows the quadrature domain Ω_Q of a node x_i and the support domain Ω_s for a gauss point x_Q. These two domains are independent and defined as $r_s = \alpha_s d_c$ and $r_Q = \alpha_Q d_c$, respectively, where α_s and α_Q are dimensionless coefficients and d_c known as characteristic length is the shortest spacing between node i and its neighbor nodes or the global boundary whichever is smaller. The number of nodal variables coupled in the Eqs. (30) and (31) changes according to the size (r_s) of the support domain Ω_s.

4.2 Discretization of the Vorticity Transport Equation

The vorticity transport equation is as follows:

$$\frac{\partial \omega}{\partial t} + u \frac{\partial \omega}{\partial x} + v \frac{\partial \omega}{\partial y} = \frac{1}{Re} \left[\frac{\partial^2 \omega}{\partial x^2} + \frac{\partial^2 \omega}{\partial y^2} \right] \qquad (32)$$

The boundary conditions are assumed to be:

$$\omega_i = \bar{\omega}_i \quad \text{on} \quad \Gamma_\omega \qquad (33)$$

$$\frac{1}{Re} \frac{\partial \omega}{\partial n} \bigg| = \bar{t}_i \qquad \text{on} \qquad \Gamma_t \qquad (34)$$

Where $\Gamma\omega$ is the essential boundary conditions, Γ_t is the Neumann boundary conditions, $\bar{\omega}$ and $\bar{t}$ are given, n is the outward unit normal vector to Γ, $\Gamma\omega$ and Γ_t are subsets of Γ satisfying $\Gamma\omega \cap \Gamma t = 0$ and $\Gamma\omega \cup \Gamma t = \Gamma$. A general local weak form of Eq. (32) by applying the weighted residual method over the quadrature domain can be written as:

$$\int_{\Omega_Q} W \left(u \frac{\partial \omega}{\partial x} + v \frac{\partial \omega}{\partial y} + \frac{\partial \omega}{\partial t} - \frac{1}{Re} \left[\frac{\partial^2 \omega}{\partial x^2} + \frac{\partial^2 \omega}{\partial y^2} \right] \right) d\Omega = 0 \qquad (35)$$

By using the divergence theorem, the following local weak form is obtained:

$$\int_{\Omega_Q} W \left(u \frac{\partial \omega}{\partial \omega} + v \frac{\partial \omega}{\partial y} \right) d\Omega$$
$$+ \frac{1}{Re} \int_{\Omega_Q} \left(\frac{\partial W}{\partial x} \frac{\partial \omega}{\partial x} + \frac{\partial W}{\partial y} \frac{\partial \omega}{\partial y} \right) d\Omega \qquad (36)$$
$$- \frac{1}{Re} \int_{\Gamma_Q} W \frac{\partial \omega}{\partial n} d\Gamma + \int_{\Omega_Q} W \frac{\partial \omega}{\partial t} d\Omega = 0$$

For the temporal discretization of the vorticity transport equation (32), a first-order backward Euler scheme is used.

$$\frac{\partial \omega}{\partial t} = \frac{\omega^n - \omega^{n-1}}{\Delta t} \tag{37}$$

By considering

$$\omega = \sum_{i=1}^{n} \phi_j \hat{\omega}_j \tag{38}$$

And enforcing the natural boundary conditions, the system equations are obtained as

$$[K]\{\hat{\omega}\} = \{f\} \tag{39}$$

where

$$[K]_{ij} = \int_{\Omega_Q} \left[u \frac{\partial \phi_j}{\partial X} + v \frac{\partial \phi}{\partial y} \right] W(X, X_i) d\Omega$$
$$+ \frac{1}{\mathrm{Re}} \int_{\Omega_Q} \left(\frac{\partial W}{\partial x} \frac{\partial \omega}{\partial x} + \frac{\partial W}{\partial y} \frac{\partial \omega}{\partial y} \right) d\Omega \tag{40}$$
$$- \frac{1}{\mathrm{Re}} \int_{\Gamma_{Qu}} W \frac{\partial \phi}{\partial n} d\Gamma - \frac{1}{\mathrm{Re}} \int_{\Gamma_{Qi}} W \frac{\partial \phi}{\partial n} d\Gamma$$
$$+ \frac{1}{\Delta t} \int_{\Omega_Q} \phi W d\Omega$$

$$\{f\}_i = \int_{\Gamma_{Qt}} W \bar{t} d\Gamma + \frac{1}{\Delta t} \int_{\Omega_Q} W \omega^{n-1} d\Omega \tag{41}$$

In order to simplify the above equation, we deliberately select a test function W such that it vanishes on Ω_Q. This can be easily accomplished by using the Heaviside step function as the weight function, with the radius r_w of the support of the weight function being replaced by the radius r_Q of the local domain Ω_Q, such that the domain integral vanishes. Using this test function and rearranging the Eqs. (42) and (43) are obtained as:

$$[K]_{i,j} = \frac{1}{\mathrm{Re}} \int_{\Gamma_{Qu}} \frac{\partial \phi_j}{\partial n} d\Gamma - \frac{1}{\mathrm{Re}} \int_{\Gamma_{Qi}} \frac{\partial \phi}{\partial n} d\Gamma$$
$$+ \frac{1}{\Delta t} \int_{\Omega_Q} \phi_j d\Omega \tag{42}$$

$$\{f\}_i = \int_{\Gamma_{Qt}} \bar{t} d\Gamma + \frac{1}{\Delta t} \int_{\Omega_Q} \omega^{n-1} d\Omega \tag{43}$$

4.3 Vorticity Boundary Condition

The vorticity boundary condition does not exist explicitly and should be constructed. The method is based on Taylor series expansion of third order. The vorticity condition can be derived from the stream function, Eq. (24). Suppose the *w* is the point at the wall, *i* is the nearest interior point to the *w* along the direction $-n_w$ (n_w is the outward unit normal to the boundary Γ at the point *w*). The distance between *w* and *i* is l. From Eq. (24), it is found that the implementation of voticity of conditions in equivalent to approximate the second-order derivatives of the stream function at the boundary, i.e. $\omega_w = \left(\partial^2 \psi / \partial l^2 \right)_w$. Taylor series expansion for ψ_i gives

$$\psi_i = \psi_w + l \left(\frac{\partial \psi}{\partial l} \right)_w + \frac{1}{2} l^2 \left(\frac{\partial^2 \psi}{\partial l^2} \right)_w$$

$$+ \frac{1}{6} l^3 \left(\frac{\partial^3 \psi}{\partial l^3} \right)_w + o(l^4) \tag{44}$$

Neglecting the terms higher than third order, and substituting the Neumann boundary condition for ψ, i. e., $\partial \psi / \partial l = 0$ (because of u = v = 0), we have

$$\left(\frac{\partial^3 \psi}{\partial l^3} \right)_w = \frac{6}{l^3} \left(\psi_i - \psi_w + \frac{l^2}{2} \omega_w \right) \tag{45}$$

Therefore

$$\omega_w = \frac{1}{4} \omega_i - \frac{3}{2l^2} \left(\psi_i - \psi_w \right) \tag{46}$$

From Eq. (46), it is found that the boundary condition for ω_w is an essential boundary condition type.

5. COMPUTATIONAL RESULTS

According to Perng and Street (1991), for its good performance for validation and simulation incompressible flows in geometrically complex domains, we choose square driven cavity flow problem as the benchmark in this research. Hence the square driven cavity flow problem is one of the most popular cases used for validation of numerical results. Also the fluid flow in a square cavity is one of the most difficult benchmark problems in flows of incompressible fluids. Therefore driven cavity flow problem is of the best benchmarks to verify numerical results. The complexity of the flow field in connection with a simple geometry makes this problem ideal for testing computational fluid dynamics codes. On the other side, the driven cavity problem can be found in a variety of important engineering applications, like flows in mixing vessels equipped with disk turbines, flows in polymer extruders and environmental flows. The problem domain with its boundary conditions is illustrated in Fig. 3. As a result the flow field is not a surface flow. Consequently the terms relating to the Froude number vanish. The imposed velocity field at the top moving wall of the cavity drives a large recirculation region inside the cavity. With increasing moving wall velocity and hence the Re number value, additional smaller recirculation zones appear in the corners of the cavity. For inspection of the computational results and showing the abilities of the Meshless Local Petrov-Galerkin (MLPG) method, the flow field in a square driven cavity was simulated using the above procedure. The results are summarized as follows:

Calculations show that, when mesh is coarse, this solution procedure shows some instability. Therefore the test case was computed on two nodal densities. The coarse mesh consisted of *30*30* nodes while the fine one consisted of *60*60* nodes (Figs. 4 and 5). For these series of calculations, only four characteristic Reynolds numbers were computed: 1000, 5000, 7500, 10000. Also, the comparison of results between the two meshes showed that the coarse mesh gave accurate results up to *Re=5000*, but was unable to give a converged

solution for *Re=10000*. It is noticed here that, for *Re=10000* with the coarse mesh consisted of *30*30* nodes no results are given but for *Re<10000*, a coarse mesh of *30*30* nodes predicts the solution with good accuracy. As *Re* increases, however, the inadequacy of coarse meshes gradually becomes apparent. The reason being that, this lower node distribution is incapable of capturing the velocity gradient within the boundary layer for *Re=10000*, resulting no stable solution. Also, as *Re* increased, very coarse meshes could not be included in the procedure. In other words when Reynolds numbers equal to and greater than 10000, the solution becomes unstable. This is due to the fact that, since the velocity gradient for *Re=10000* is greater than that for *Re=7500*,and also since the boundary layer for *Re=10000* is thinner compared to that for *R e = 7 5 0 0* , t o obtain a stable solution at *Re=10000*, the number of nodes must be increased and a *30*30* node distribution is not enough. Hence for *Re =10,000*, the fine mesh was used. Therefore numerical simulations were performed on the mesh of *60*60* nodes. Finally, for higher Reynolds number, full convergence was obtained. On the other hand, the definition of convergence in the fine meshes appears to influence the final solution obtained. Therefore more precisely, for Reynolds numbers up to 5000, a fine mesh of *60*60* was used. Also, In order to accurately resolve high gradients of velocities and vorticities, the fine mesh have to be used.
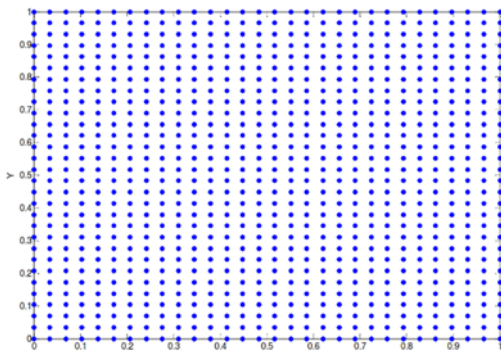
Fig. 4. Computational nodal density for driven cavity: (*30*30*).
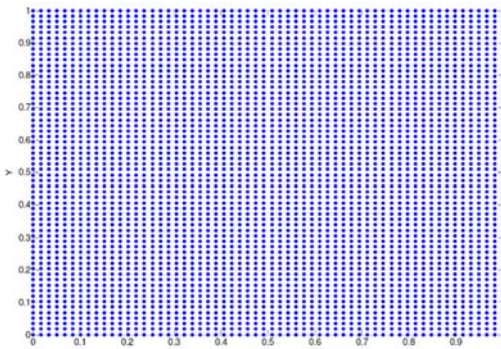
Fig. 5. Computational nodal density for driven cavity: (*60*60*).

In fact, the employment of fine mesh is popular, particularly for simulation of the flow field at higher Reynolds numbers. As seen from Fig. 6 to Fig. 13, the fine mesh solutions exhibit additional vortices in or near the cavity corners as Re increases. It should be noted that the fine mesh solutions have been obtained very efficiently for high-Re flow using the Meshless Local Petrov-Galerkin (MLPG) method and vorticity-stream function formulation. Therefore the fine mesh parameter in this procedure is considered very important. Finally, in view of the above remarks, the present fine mesh should be very useful.
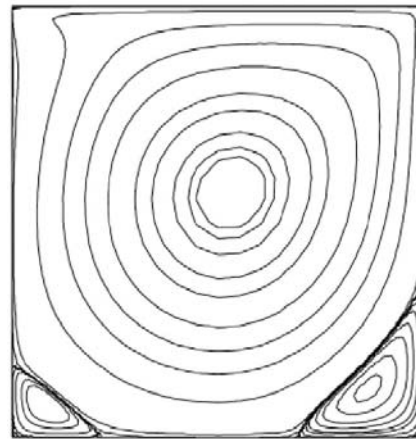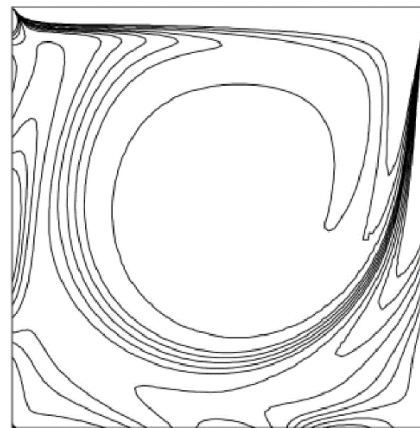

Fig. 6. Streamlines for *Re=1000*.

Fig. 7. Vorticity isolines for *Re=1000*.

The computations were performed for different Reynolds numbers, *Re=1000, Re=5000, Re=7500* and *Re=10000*, with the characteristic length, *L=1m*, and characteristic velocity, *U =1m/s,* and the no-slip and impermeable wall boundary conditions are imposed along the remaining walls (Figs. 6–19). All computations were performed by time stepping procedure, where the typical time steps were Δ*t=1* for *Re=1000* and *Re=5000* and Δ*t=0.1* for *Re=7500* and *Re=10000* (Figs. 6–15). From Fig. 6 to Fig. 13, the streamlines and vorticity contours for different Reynolds numbers, computed is shown, with the expected behavior. As it is shown in those Figs., there are no oscillations in the streamlines even at high Reynolds numbers. On the other hand, as shown in Figs. 6, 8, 10 and 12 in general, a two to four vortex structure is found depending on the

Reynolds number used. The pattern of the flow changes from two-vortex structure at low speeds to four -vortex structure at high speeds, as shown in Figs. 6, 8, 10 and 12. Hence, a two and four-vortex structure is analyzed and good results are claimed. In addition, the comparison of velocity profiles along the lines $x = 0.5$ and $y = 0.5$, is presented in Figs. 14 and 15. Reference (Ghia *et al.* 1982), is a classic benchmark, extensively used for comparison. In this reference, streamline-vorticity scheme is used and calculations for Reynolds number up to 10,000 are computed, showing good agreement with available data. As shown in Figs. 14 and 15 the results of the computations are compared with the results of Ghia (1982) obtained by the FDM. In other words from Fig. 14 to Fig. 15, both velocity components and their comparison with the classical results of Ghia are shown. It is observed that the obtained results agreed very well with the classical results of Ghia. In other words as shown in Figs. 14 and 15 for different Reynolds numbers, the agreement is excellent. As seen from Fig. 6 to Fig. 13, the fine mesh solutions exhibit additional vortices in or near the cavity corners as Re increases. Also, in Figs. 16 – 19, the pressure field is presented for different Reynolds numbers. It should be noted that as seen from Fig. 16 to Fig. 19, at the top and right side of the cavity, due to the intense flow variations, there exist intensive pressure variations. The pressure field, at this location, shows an expansion, while at the left edge a compression is observed.
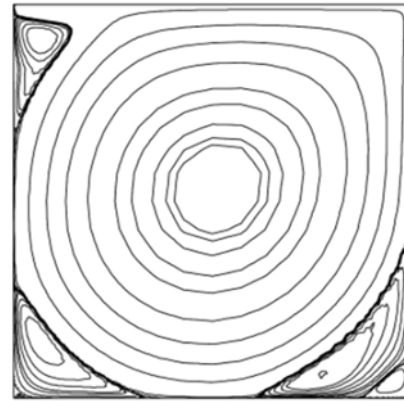

Fig. 10. Streamlines for *Re=7500*.
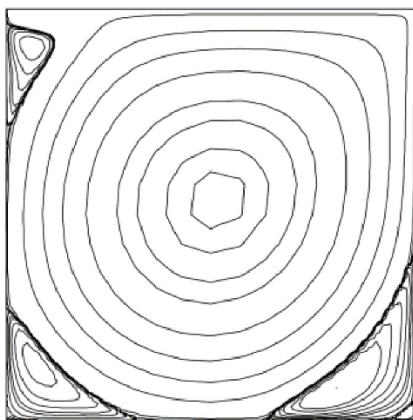

Fig. 11. Vorticity isolines for *Re=7500*.
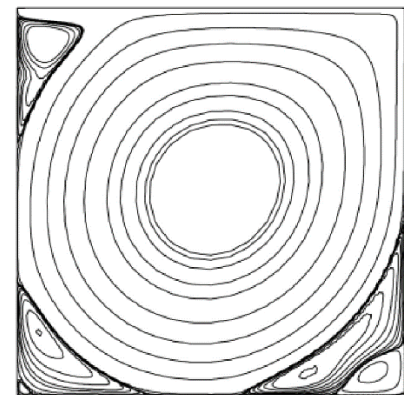

Fig. 8. Streamlines for *Re=5000*.

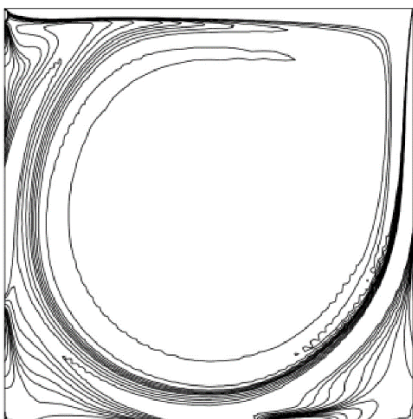**Fig. 12. Streamlines for *Re=10000*.**

Fig. 9. Vorticity isolines for *Re=5000*.
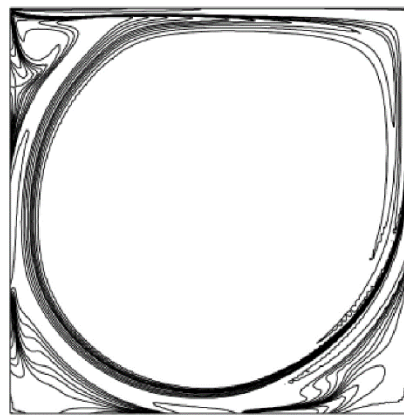

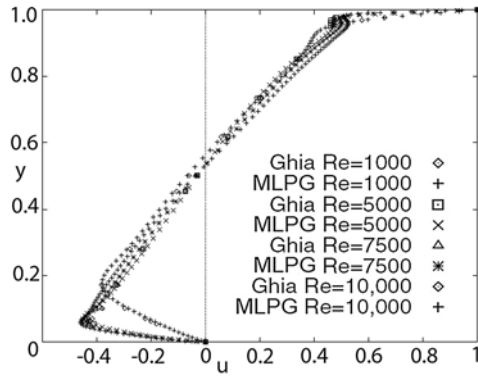**Fig. 13. Vorticity isolines for *Re=10000*.**

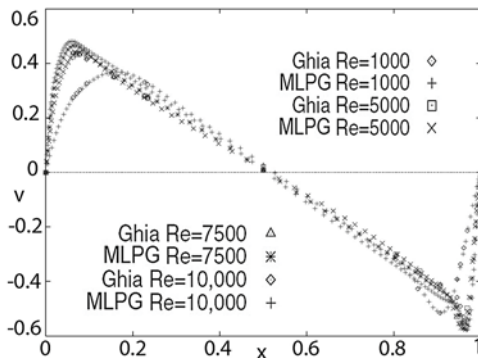**Fig. 14. Comparison of u velocity profiles at x=0.5.**

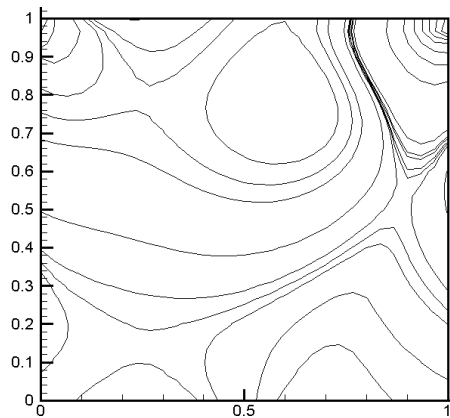**Fig. 15. Comparison of v velocity profiles at y=0.5.**
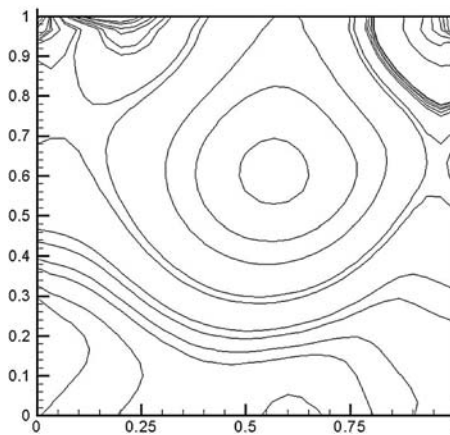

Fig. 16. Pressure distribution for *Re=100*.

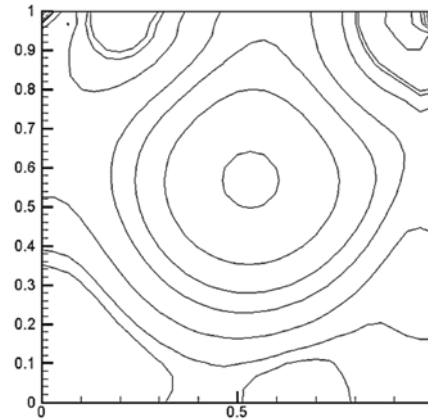
Fig. 17. Pressure distribution for *Re=400*.

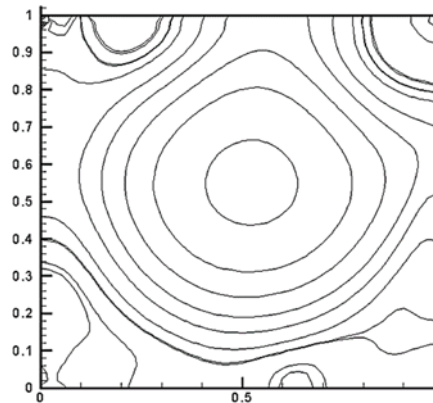**Fig. 18. Pressure distribution for *Re=1000*.**

Fig. 19. Pressure distribution for *Re=2000*.

6. CONCLUSION

In the present article, a numerical algorithm is presented for computation of unsteady incompressible flows, governed by the Navier–Stokes equations in vorticity-stream function formulation. In other words, a numerical algorithm using the MLPG is extended and accurate calculations are claimed for different Reynolds numbers. A local multiquadrics RBFs technique using radial basis functions is used to construct the trial function entirely in terms of a set of scattered nodes. By using multiquadrics RBFs the nodes are treated according to their distances and not their coordinates. It can be seen that no special treatment is needed to impose the essential boundary conditions. The present method is based on a local weighted residual method with the Heaviside step function as the test function over a local subdomain. Therefore in this research in order to avoid the evaluation of any numerical integration in the weak form, the Heaviside step test function is chosen as the test function in each sub-domain. The efficiency; accuracy and robustness of the numerical algorithm are demonstrated by the standard driven cavity. The comparison of computational results with the results of Ghia shows that the present numerical algorithm is capable of accurate resolution of flow fields in complex geometries. Therefore the ability and accuracy of the MLPG

was presented by solving the standard driven cavity flow problem with reasonable accuracy when compared to solutions obtained by Ghia. In other words the benchmark computations indicate that the MLPG is very effective in the simulation of fluid flow problems. Finally, the consequence is that the present numerical algorithm should be very useful.

REFERENECES

Alam, M. M. A., T. Setoguchi M. Takao and H. D. Kim (2016). Numerical analysis of the high speed driven cavity flow in 2-d curved channel. *Journal of Applied Fluid Mechanics* 9(2), 529-536.

Atluri, S. N. and S. Shen (2002). The meshless local Petrov-Galerkin (MLPG) method: a simple and less-costly alternative to the finite element and boundary element methods. *Computer Modelling in Engineering and Sciences* 3(1), 11-52.

Atluri, S. N. and Zhu, T. (1998a). A new meshless local Petrov-Galerkin (MLPG) approach in computational mechanics. *Computational Mechanics* 22(2), 117-127.

Atluri, S. N., and T. Zhu (1998b). A new meshless local Petrov-Galerkin (MLPG) approach to non-linear problems in computer modelling and simulation. *Computational Modeling and Simulation in Engineering* 3(3), 187-196.

Babuska, I., and J. M. Melenk (1997). The partition of unity method. *International Journal for Numerical Methods in Engineering* 40(4), 727-758.

Belytschko, T., Y. Krongauz, D. Organ and W. K. S. Liu (1996). Smoothing and accelerated computations in the element free Galerkin method. *Journal of Computational and Applied Mathematics* 74, 111-126.

Belytschko, T., Y. Y. Lu and L. Gu (1994). Element Free Galerkin Methods. *International Journal for Numerical Methods in Engineering* 37(2), 229-256.

Bunsri, T., M. Sivakumar and D. Hagare (2008). Numerical modelling of tracer transport in unsaturated porous media. *Journal of Applied Fluid Mechanics* 1(1), 62-70.

Chen, R., S. Shao, X. Liu and X. Zhou (2015). Applications of shallow water SPH model in mountainous rivers. *Journal of Applied Fluid Mechanics* 8(4), 863-870.

De, S. and J. Bathe (2000). The method of finite spheres. *Comput. Mech.* 25, 329-345.

Dolbow, J. and T. Belytschko (1998). An introduction to programming the meshless element- free Galerkin method. *Archives of Computational Methods in Engineering* 5(3), 207-241.

Frank, R. (1982). Scattered data interpolation: testsof some method. *Mathematics of Computation* 38(157), 181-200.

Ghia, U., K. N. Ghia and C. T. Shin (1982). High-resolution for incompressible flow using the Navier-Stokes equation and a multigrid method. *Journal of Computational Physics* 48(3), 387-411.

Gu, Y. T. and G. R. Liu (2001). A meshless local Petrov-Galerkin (MLPG) formulation for static and free vibration analyses of thin plates. *Computer Modelling in Engineering and Sciences* 2(4), 463-476.

Gu, Y. T. and G. R. Liu (2001). Meshless local Petrov-Galerkin (MLPG) method for free and forced vibration analyses for solids. *Computational Mechanics* 27(3), 188–198.

Hardy, R. L. (1990). Theory and applications of themutliquadrics –biharmonic method (20 Years of Discovery 1968–1988). *Computers and Mathematics with Applications* 19, 163–208.

Harichandan, A. B. and A. Roy (2012). CFR: A finitevolume approach for computing incompressible viscous flow. *Journal of Applied Fluid Mechanics* 5(3), 39-52.

Jafari, M. J., A. Karimi, A. E. Usachov and H. KananiMoghaddam (2011). The fire simulation in a road tunnel. *Journal of Applied Fluid Mechanics* 4(1), 121-138.

Kansa, E. J. (1990). Multiquadrics a scattered data approximation scheme with applications to computational fluid dynamics, part I. *Computers and Mathematics with Applications* 19, 127-145.

Lin, H. and S. N. Atluri (2001). The meshless local Petrov-Galerkin (MLPG) method for solving incompressible Navier–Stokes equations. *Computer Modelling in Engineering and Sciences* 2(2), 117–142.

Liu, G. R. (2003). *Mesh free methods: moving beyondthe finite element method*, 1st ed. Boca Raton, FL: CRC Press.

Liu, W. K., S. Jun and Y. F. Zhang (1995). Reproducing kernel particle methods. *International Journal for Numerical Methods in Fluids* 20, 1081–1106.

Lu, Y. Y., T. Belytschko and L. Gu (1994). a new implementation of the element free Galerkin method. *Computer Methods in Applied Mechanics and Engineering* 113, 397-414.

Monaghan, J. J. (1992). Smooth particle hydrodynamics. *Annual Review of Astronomy and Astrophysics* 30, 543-574.

Perng, C. Y. and R. L. Street (1991). A coupled multigrid-domain-splitting technique for simulating incompressible flows in geometricallycomplex domains. *International Journal for Numerical Methods in Fluids* 13, 269-286.

Saeedpanah, I., E. Jabbari and M. A. Shayanfar (2011). Numerical simulation of groundwater flow via a new approach to the local radial point interpolation meshless method. *International Journal of Computational Fluid Dynamics* 25(1), 17-30.

Shirani, E., F. Ghadiri and A. Ahmadi (2011). Modeling and simulation of interfacial turbulent flows. *Journal of Applied Fluid Mechanics* 4(2), Special Issue, 43-49.

Sukumar, N., B. Moran and B. Belytschko (1998). The natural element method in solid mechanics. *International Journal for Numerical Methods in Engineering* 43(5), 839-887.

Zhu, T., J. D. Zhang and S. N. Atluri (1998). A meshless local boundary integral equation (LBIE) method for solving nonlinear problems. *Computational Mechanics* 22(2), 174-186.